TEM Investigation of the Domain Structure in Prototype Antiferroelectric Perovskites

Zhongming Fan¹, Tao Ma², Jing Wei³, Tongqing Yang³, and Xiaoli Tan^{1*}

Abstract

The domain structure is comprehensively investigated in the prototype antiferroelectric perovskite PbHfO₃ using transmission electron microscopy. The antiparallel Pb-displacements, and the one {110}_c-atomic-plane and four {110}_c-atomic-plane (subscript c denotes the pseudocubic notation) polar translational boundaries within antiferroelectric domains are directly revealed. Various antiferroelectric domain structures are observed, among which a new "cloverleaf pattern" domain morphology is discovered in PbHfO₃. In another prototype antiferroelectric perovskite PbZrO₃, antiferroelectric domains appear to favor the "lamellar pattern". The combination of these two patterns makes even more complicated domain structures in PbZrO₃.

¹ Department of Materials Science and Engineering, Iowa State University, Ames, IA 50011, USA

² Ames Laboratory, U.S. Department of Energy, Ames, IA 50011, USA

³ School of Materials Science and Engineering, Tongji University, Shanghai 201804, China

This work was supported by the National Science Foundation (NSF) through Grant DMR-1700014.

^{*}Member, the American Ceramic Society.

Author to whom correspondence should be addressed. Electronic mail: xtan@iastate.edu

I. INTRODUCTION

Antiferroelectric (AFE) ceramics have received growing attention for their attractive energy storage capacity. ¹⁻⁵ In addition to identifying compositions for a higher energy density, studies on fundamental issues in AFE ceramics also regain widespread interest. Among the prototype AFE perovskite compounds of PbZrO₃, PbHfO₃, and NaNbO₃, ⁶ PbHfO₃ is the least studied due to the fabrication difficulty. ⁷⁻¹⁰ Even for PbZrO₃ and NaNbO₃, investigations are not as comprehensive as other ferroelectric (FE) compounds and primarily devoted to the AFE↔FE phase transition of their solid solutions. ¹¹⁻¹³ Several basic issues, such as dipole arrangement, domain wall crystallography, and domain configuration, have been overlooked in these prototype AFE perovskite compounds.

It should be noted that these mentioned issues in FE crystals are relatively clear to the community. Depending upon the crystal structure, the dipoles in two neighboring FE domains (within each of which are aligned to the same direction) can form different angles across the domain wall. For instance, 71° or 109° are unique to rhombohedral FE crystals where the dipole is along the pseudo-cubic <111>c direction (subscript c denotes the pseudo-cubic notation); 60° or 120° are observed in orthorhombic FE phase; while 90° is preferred in tetragonal crystals. In FE polycrystalline ceramics, each grain contains many domains and they form complex patterns like the lamellar pattern, the herringbone pattern, or their combinations. 15,16

In prototype AFE perovskite compounds, the dipoles (in the form of cation displacements) are aligned antiparallel within one domain, and the most reported are 90° AFE domains although 60° and 120° walls are both possible because of the orthorhombic symmetry. ^{17,18} Complex domain morphologies at the sub-grain length scale have ever been discussed only in NaNbO₃-based ceramics. ¹⁹⁻²¹ Even though transmission electron microscopy (TEM) has been regarded as

one of the most suitable tools for domain structure analysis, detailed TEM investigation on PbHfO₃ has not yet been reported.²² In the meantime, domain walls have been imaged with TEM in PbZrO₃,^{23,24} but its complex AFE domain morphology has never been analyzed. In this work, thorough TEM studies are conducted to clarify the dipole arrangement and domain structure in prototype AFE compounds of PbHfO₃ and PbZrO₃.

II. EXPERIMENTAL PROCEDURE

Polycrystalline ceramic of PbHfO₃ was prepared using the rolling process method while PbZrO₃ ceramic pellets were processed by the solid-state reaction method. The detailed preparation procedure has been reported in our previous works.^{4,25}

As-sintered ceramic pellets were mechanically ground and polished down to a thickness of 120 µm, and then ultrasonically cut into disks with a diameter of 3 mm. After dimpling and polishing, the disks were annealed at 200 °C for 2 hours and Ar-ion milled until perforation. Diffraction contrast analysis of domain structure was conducted with a FEI Tecnai G2-F20 TEM. High resolution atomic imaging was performed using a FEI Titan Themis 300 probe-corrected scanning transmission electron microscopy (STEM) at an accelerating voltage of 200 kV. High-angle annular dark-field (HAADF) images were captured using a sub-angstrom electron probe with a convergence angle of 18 mrad and a detection angle of 99–200 mrad. The method for Pb-displacement mapping was described in our previous work.²⁵

III. RESULTS AND DISCUSSION

(1) 90° AFE domain wall

Figure 1(a) shows a grain in polycrystalline PbHfO₃ viewed along its <001>c zone-axis, with two large 90° AFE domains and a curved domain wall. The selected area electron diffraction (SAED) pattern recorded from the domain wall region (inset in Fig. 1a) displays two perpendicular sets of ¼{110}c superlattice diffraction spots. Since PbHfO₃ is isostructural with PbZrO₃ at room temperature, presumably can be considered as a commensurately modulated structure with a modulation wavelength of four {110}c atomic planes, leading to the presence of ¼{110}c superlattice diffraction spots. The modulation manifests itself as the Pb-displacement along the <110>c direction. To minimize the electrostatic energy, the 90° AFE domain wall is expected to be on {100}c planes, at least locally. As a result, it should be edge-on when viewed along the <001>c zone-axis. As can be seen in Fig. 1(a), the domain wall has a sharp contrast, confirming its edge-on position.

The local dipole arrangement in each domain is mapped out through calculating the off-center displacement of Pb from the HAADF images. Figure 1(b) and 1(c) shows the results in the upper and the lower domain, respectively. Not only the <110>c direction of Pb-displacement, but also the antiparallel arrangement of the resulting dipoles (represented by the arrows) have been directly revealed and verified. Furthermore, the modulation stripes, which give rise to the ½{110}c-atomic-plane thick alternate in the Pb-displacement, and those in one domain are perpendicular to those in the other domain across the 90° AFE domain wall. However, there exist exceptions when a stripe contains either four or only one {110}c atomic planes (highlighted with the red dashed line). These stripes are essentially two types of polar translational boundary, which appear as the straight line features in the upper domain in the bright-field micrograph in Fig. 1(a). It should be noted that

these line features are also observed in the lower domain (with an orientation perpendicular to those in the upper domain) under a slightly different tilting condition.

(2) Non-90° AFE domain walls

Another type of AFE domain wall in PbHfO₃ viewed along <001>_c zone-axis is displayed in Fig. 2. The SAED patterns indicate that one domain displays one set of ¼{110}_c superlattice spots while the other domain exhibits only the fundamental diffraction spots. The absence of ¼{110}_c superlattice spots in an AFE domain indicates that the modulation stripes in that domain are not viewed edge-on. Moreover, the domain wall is also not edge-on but inclined to the viewing direction. Such a configuration of AFE domains can be interpreted in terms of non-90° domains.

Following the scheme of domain configurations in orthorhombic FE crystals, domains in orthorhombic AFE crystals can also form 60° or 120° domain structures. If only straight domain walls are considered, 60° and 120° domain walls are preferred to be on {110}c and {112}c planes, respectively (illustrated in the first row of Fig. 3). In the second row of Fig. 3, possibilities for <001>c zone-axis observation are listed. Two configurations, "60° domains viewed along [001]c" and "120° domains viewed along [100]c", match the situation shown in Fig. 2 with an inclined domain wall and superlattice spots in one domain. Further discerning between the two possibilities can be made based on the trace direction of the domain wall in the micrograph. The first possibility corresponds to a [100]c trace, hence, can be excluded.

Therefore, the domains shown in Fig. 2 are likely to be 120° AFE domains. However, this domain wall is not linear either. Instead, it contains three segments, which means that these two 120° AFE domains are separated by multiple walls. Such curved domain walls are quite common in AFE perovskites (see both Fig. 1 and 2), while the detailed structure, such as the dipole

arrangement at the joint or the interaction with polar translational boundaries, will be examined elsewhere.²⁸

In addition to the <001>c zone-axis, <111>c zone-axis is also suitable for analyzing domain structures in orthorhombic AFE crystals, of which the observation possibilities are listed in the third row of Fig. 3. Figure 4 demonstrates how to determine the domain wall type based on <111>c zone-axis observations in PbHfO₃. As shown in Fig. 4a, the edge-on domain wall is indexed to be {110}c plane while the diffraction pattern recorded from the domain wall region displays two sets of ¼{110}c superlattice spots. Comparing with configurations in the third row of Fig. 3 suggests that the only matching possibility is "60° domains viewed along [111]c".

As shown in Fig. 1 under the <001>c zone-axis, the Pb-displacements are mapped out so that the angle between dipoles in two neighboring domains can be directly measured (Fig. 1). It should be pointed out that such mapping is no longer feasible along the <111>c zone-axis because Hf and Pb will overlap in atomic columns (Fig. 4b). There exists an alternative approach to reveal the modulation stripe's orientation within AFE domains, but is incapable of providing the dipole vectors. Based on the HAADF image, geometric phase analysis (GPA) calculates and illustrates the deviation of a real local lattice with respect to a reference lattice generated from the electron diffraction pattern. As can be seen in Fig. 4b, the stripes (represented by the color contrast) form a 120° angle across the domain wall, in consistence with the indication from each domain's superlattice diffraction spots. In the "60° domains viewed along [111]c" configuration (Fig. 3), the angle between the projections of the dipoles from neighboring domains indeed appears as 120°. As a result, the observed domain wall in Fig. 4 is determined to be of 60° type.

(3) Complex AFE domain morphologies

Having Fig. 3 as guidance, it should be ready to analyze complex domain morphologies in grains which contain more than two domains. In the present study, three typical morphologies are found in PbHfO₃ and PbZrO₃, including cloverleaf pattern, lamellar pattern and the combination of them.

Figure 5 displays a grain in PbHfO₃ viewed along the <111>c zone-axis. The grain of interest contains three large domains and the domain walls are marked with yellow dashed lines. The SAED patterns recorded from each domain show distinct sets of ½{110}c superlattice spots. Known from the bright-field micrograph and the diffraction patterns, domains 1 & 2 have an edge-on {110}c wall in between and the projection angle of dipoles is 120°, which is identical with the situation in Fig. 4. So, domains 1 & 2 are 60° AFE domains. Similarly, domains 1 & 3 are 60° AFE domains as well. However, the wall between domains 2 & 3 is inclined with the surface trace along the <110>c direction and the projection angle of dipoles is 60°. According to Fig. 3, they are 120° AFE domains (the "[111]c" possibility). Apart from the straight domain walls, these three domains converge to a point in the center (position 4) where the diffraction pattern shows all three sets of ¼{110}c superlattice spots. Therefore, such a morphology is named as cloverleaf pattern.³⁰

Figure 6 displays the lamellar AFE domain pattern found in PbZrO₃. Unlike the cloverleaf pattern comprising three leaves, the number of lamella that the pattern contains can vary from grain to grain. A four-lamella pattern in a <001>c aligned grain is shown in Fig. 6(a). Domains 1 & 3 have one set of ½{110}c superlattice spots while domains 2 & 4 show nothing but the fundamental spots. Moreover, none of the domain walls are edge-on but their traces are roughly along the same <102>c direction. According to Fig. 3, these domain walls should be 120° walls of the "[100]c" possibility. Figure 6(b) shows another lamellar pattern containing six lamellae

viewed along the $<111>_c$ zone-axis. Domains 1 & 3 & 5 have the same set of $\frac{1}{4}\{110\}$ superlattice spots while domains 2 & 4 & 6 have another set. The projection angle of dipoles between every two neighboring domains is 120° . The edge-on domain walls are on parallel $\{110\}_c$ planes. Hence, all the walls are 60° type of the " $[1\overline{1}1]_c$ " possibility.

Not only the increase in the number of lamella is commonly seen in the lamellar pattern, but also the combination of the cloverleaf and lamellar AFE domain patterns is observed for increased complexity of AFE domain morphology. One example is found in PbZrO₃ (Fig. 7). Viewed along the <001>c zone-axis, a lamellar pattern with seven lamellae occupies the grain. The parallel domain walls are all edge-on on the {110}c planes and none of these seven domains shows any superlattice spots (exemplified by domains 1 & 3). The configuration corresponds to the "60° domains viewed along [100]c" possibility in Fig. 3. Additionally, a cloverleaf pattern is present in the upper right of the grain. Domain 2 shows one set of ¼{110}c superlattice spots and forms an 120° angle with domain 1 or 3 (schematically illustrated here). Conceivably, the domain morphology could become even more complicated after including more cloverleaf sections or involving the curved domain walls.

It needs to be clarified that the only type of complex domain morphology found in PbHfO₃ is cloverleaf pattern, while lamellar patterns are ubiquitous in PbZrO₃. It is well known that the equilibrium domain morphology is dictated by the balance between the depolarization energy within the domain and energy associated with the domain wall.³¹ For AFEs, depolarization energy can be ignored due to the compensated polarization of antiparallel dipoles. Thereby domain wall energy should play a crucial role in domain morphology formation. In cloverleaf patterns, the complicated intersections of three domain walls (Figs. 5 and 7) inevitably introduce additional energy in comparison with lamellar patterns. Thus, the absence of lamellar patterns in

PbHfO₃ might have its energetic origin, which requires *ab initio* calculations focusing on the effects of the B-site cation in the ABO₃ perovskite crystal. Such effects are also manifested in the type of polar translational boundaries (Fig. 1). In PbZrO₃, four {110}_c-atomic-plane boundaries are seldom.²⁸ The presence of the four {110}_c-atomic-plane boundaries in PbHfO₃ may have its origin of Hf on the B-site.

IV. CONCLUSIONS

The antiparallel dipole arrangement in PbHfO₃ is directly visualized at the atomic level. Two types of polar translational boundaries are also discerned. At the sub-grain spatial range, a systematic analysis of the type of AFE domain walls (60°, 90° or 120°) is reported. With the assistance of such analysis, complex domain morphologies are elucidated in both PbHfO₃ and PbZrO₃. A new cloverleaf AFE domain pattern is discovered in PbHfO₃ while the lamellar pattern dominates in PbZrO₃.

ACKNOWLEDGEMENTS

The National Science Foundation (NSF), through Grant No. DMR-1700014, supported the microscopic work (Z. Fan, T. Ma & X. Tan). The ceramic processing (J. Wei & T. Yang) is supported by National Natural Science Foundation of China (No. 51472181).

- 1. Chauhan A, Patel S, Vaish R, Bowen CR. Anti-ferroelectric ceramics for high energy density capacitors. Materials 2015;8:8009.
- 2. Zhao L, Liu Q, Gao J, Zhang S, Li J. Lead-free antiferroelectric silver niobate tantalate with high energy storage performance. Adv. Mater. 2017;29:1701824.
- 3. Hao X, Zhai J, Yao X. Improved energy storage performance and fatigue endurance of Srdoped PbZrO₃ antiferroelectric thin films. J. Am. Ceram. Soc. 2009;92:1133.
- 4. Wei J, Yang T, Wang H. Excellent energy storage and charge-discharge performances in PbHfO₃ antiferroelectric ceramics. J. Euro. Ceram. Soc. 2019;39:624.
- 5. Wang H, Liu Y, Yang. T, Zhang. S. Ultrahigh energy-storage density in antiferroelectric ceramics with field-induced multiphase transitions, Adv. Funct. Mater. 2018; 1807321.
- 6. Hao X, Zhai J, Kong LB, Xu Z. A comprehensive review on the progress of lead zirconate-based antiferroelectric materials. Prog. Mater. Sci. 2014;63:1.
- 7. Shirane G, Pepinsky R. Phase transitions in antiferroelectric PbHfO₃. Phys. Rev. 1953;91:812.
- 8. Samara GA. Pressure and temperature dependence of the dielectric properties and phase transitions of the antiferroelectric perovskites: PbZrO₃ and PbHfO₃. Phys. Rev. B 1970;1:3777.
- 9. Corker DL, Glazer AM, Kaminsky W, Whatmore RW, Dec J, Roleder K. Investigation into the crystal structure of the perovskite lead hafnate, PbHfO₃. Acta Crystallogr. B 1998;54:18.
- 10. Huband S, Glazer AM, Roleder K, Majchrowski A, Thomas PA. Crystallographic and optical study of PbHfO₃ crystals. J. Appl. Crystallogr. 2017;50:378.
- 11. Guo H, Tan X. Direct observation of the recovery of an antiferroelectric phase during polarization reversal of an induced ferroelectric phase. Phys. Rev. B 2015;91:144104.

- 12. Tan X, Ma C, Frederick J, Beckman S, Webber KG. The antiferroelectric ferroelectric phase transition in lead-containing and lead-free perovskite ceramics. J. Am. Ceram. Soc. 2011;94:4091.
- 13. Viehland D, Forest D, Xu Z, Li JF. Incommensurately modulated polar structures in antiferroelectric Sn-modified lead zirconate titanate: the modulated structure and its influences on electrically induced polarizations and strains. J. Am. Ceram. Soc. 1995;78:2101.
- 14. Guo H, Voas BK, Zhang S, Zhou C, Ren X, Beckman SP, Tan X. Polarization alignment, phase transition, and piezoelectricity development in polycrystalline
 0.5Ba(Zr_{0.2}Ti_{0.8})O₃-0.5(Ba_{0.7}Ca_{0.3})TiO₃. Phys. Rev. B 2014;90:014103.
- 15. Ricote J, Whatmore RW, Barber DJ. Studies of the ferroelectric domain configuration and polarization of rhombohedral PZT ceramics. J. Phys. Condens. Matter 2000;12:323.
- 16. Woodward DI, Knudsen J, Reaney IM. Review of crystal and domain structures in the PbZr_xTi_{1-x}O₃ solid solution. Phys. Rev. B 2005;72:104110.
- 17. Tanaka M, Saito R, Tsuzuki K. Electron microscopic studies on domain structure of PbZrO₃. Jpn. J. Appl. Phys. 1982;21:291.
- 18. Shen GJ, Shen K. Electron microscope study of domains in PbZrO₃. J. Mater. Sci. 1999;34:5153.
- Gao L, Guo H, Zhang S, Randall CA. A perovskite lead-free antiferroelectric xCaHfO₃-(1-x)NaNbO₃ with induced double hysteresis loops at room temperature. J. Appl. Phys. 2016;120:204102.
- 20. Shimizu H, Guo H, Reyes-Lillo SE, Rabe KM, Randall CA. Lead-free antiferroelectric: $xCaZrO_3-(1-x)NaNbO_3$ system ($0 \le x \le 0.10$). Dalton Trans. 2015;44:10763.

- 21. Yamazoe S, Sakurai H, Saito T, Wada T. Observation of domain structure in 001 orientated NaNbO₃ films deposited on (001) SrTiO₃ substrates by laser beam scanning microscopy. Appl. Phys. Lett. 2010;96:092901.
- 22. Madigout V, Baudour JL, Bouree F, Favotto C, Roubin M, Nihoul G. Crystallographic structure of lead hafnate (PbHfO₃) from neutron powder diffraction and electron microscopy. Philos. Mag. A 1999;79:847.
- 23. Xu Z, Dai X, Viehland D, Payne DA. Ferroelectric domains and incommensuration in the intermediate phase region of lead zirconate. J. Am. Ceram. Soc. 1995;78:2220.
- 24. Tanaka M, Saito R, Tsuzuki K. Determinations of Space Group and Oxygen Coordinates in the Antiferroelectric Phase of Lead Zirconate by Conventional and Convergent-Beam Electron Diffraction. J. Phys. Soc. Jpn. 1982;51:2635.
- 25. Ma T, Fan Z, Xu B, Kim TH, Ballaiche L, Kramer MJ, Tan X, Zhou L. Uncompensated polarization in incommensurate modulations of perovskite antiferroelectrics. Phys. Rev. Lett. 2019; submitted.
- 26. Wei XK, Chia CL, Roleder K, Setter N. Polarity of translation boundaries in antiferroelectric PbZrO₃. Mater. Res. Bull. 2015;62:101.
- 27. Wei XK, Vaideeswaran K, Sandu CS, Chia CL, Setter N. Preferential creation of polar translational boundaries by interface engineering in antiferroelectric PbZrO₃ thin films. Adv. Mater. Interfaces 2015;2:1500349.
- 28. Ma T, Fan Z, Tan X, Zhou L. Atomically resolved domain boundary structure in lead zirconate-based antiferroelectrics. Mater. Res. Lett. 2019; in preparation.

- 29. Zhu Y, Ophus C, Ciston J, Wang H. Interface lattice displacement measurement to 1pm by geometric phase analysis on aberration-corrected HAADF STEM images. Acta Mater. 2013;61:5646.
- 30. Choi T, Horibe Y, Yi HT, Choi YJ, Wu W, Cheong SW. Insulating interlocked ferroelectric and structural antiphase domain walls in multiferroic YMnO₃ Nat. Mater. 2010;9:253.
- 31. Shih WY, Shih WH, Aksay IA. Size dependence of the ferroelectric transition of small BaTiO₃ particles: Effect of depolarization. Phys. Rev. B 1994;50:15575.

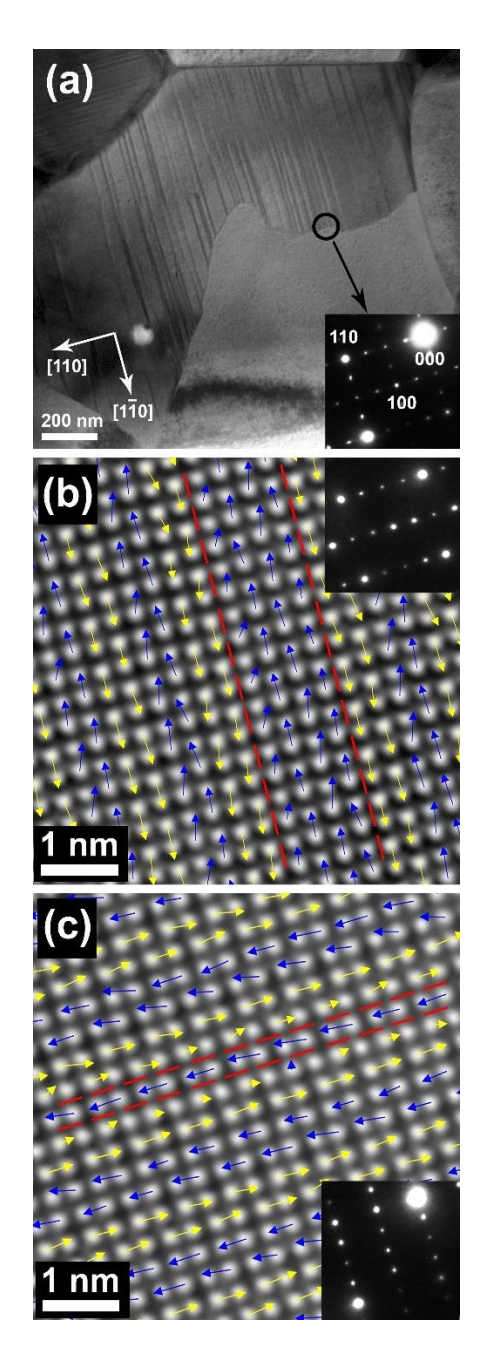


Fig. 1. (a) A curved 90° domain wall of PbHfO₃ viewed along <001> zone-axis. The inset shows the diffraction pattern recorded from the domain wall region. (b) The dipole arrangement mapping based on a HAADF-STEM image taken from the upper domain. The red dashes lines highlight a four-layers polar translational boundary. (c) The dipole arrangement mapping based on a HAADF-STEM image taken from the lower domain. The red dashes lines highlight a one-layer polar translational boundary.

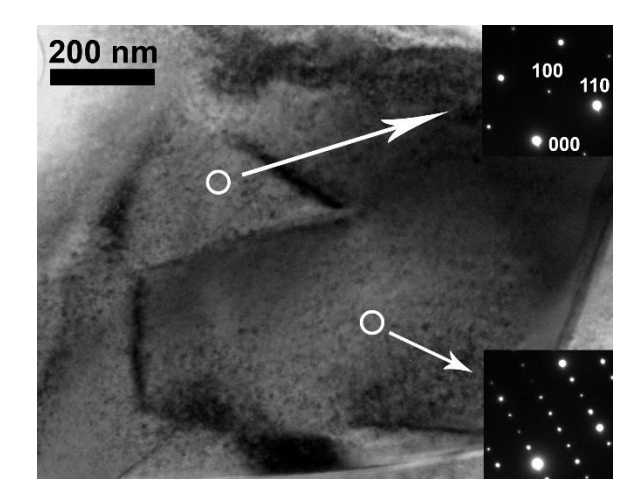


Fig. 2. A non-90° domain wall of PbHfO₃ viewed along <001> zone-axis. Two insets show the diffraction patterns recorded from corresponding domains.

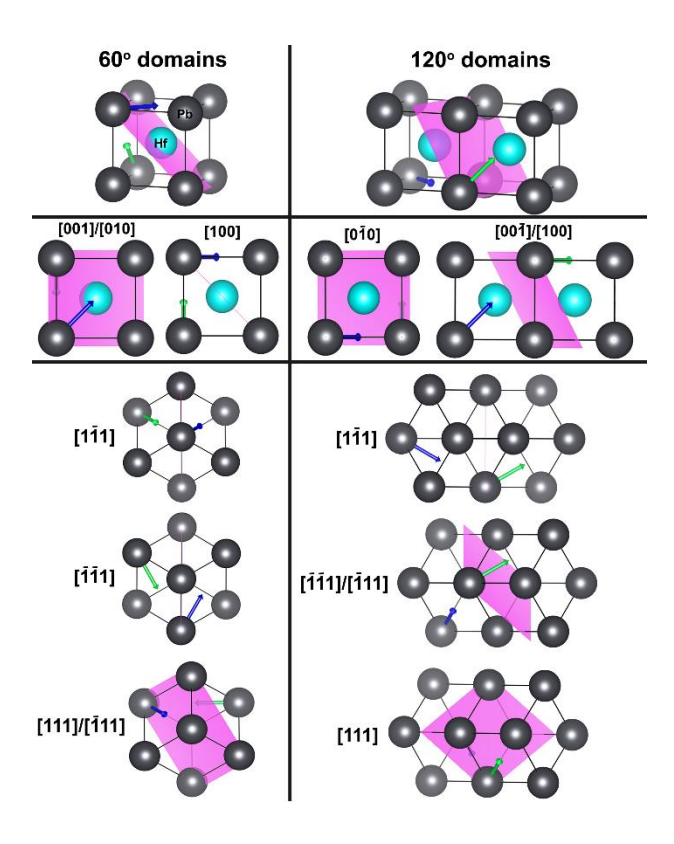


Fig. 3. List of possibilities for a $60^{\circ}/120^{\circ}$ domain wall viewed along different <001> and <111> zone axes.

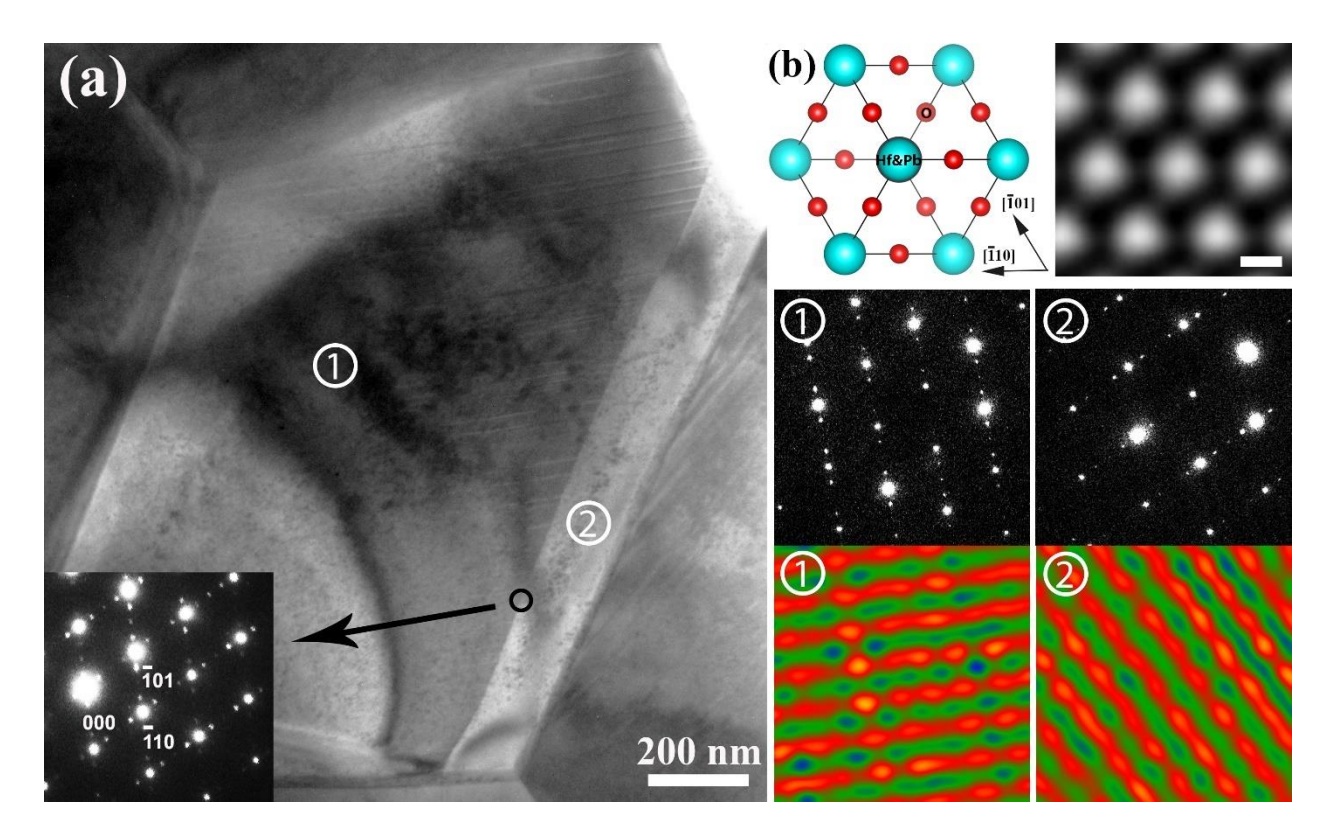


Fig. 4. (a) A straight 60° domain wall of PbHfO₃ viewed along <111> zone-axis. The inset shows the diffraction pattern recorded from the domain wall region. (b) Orientation of the stripes in corresponding domains revealed by HAADF-STEM-GPA. The scale bar represents 2 angstroms.

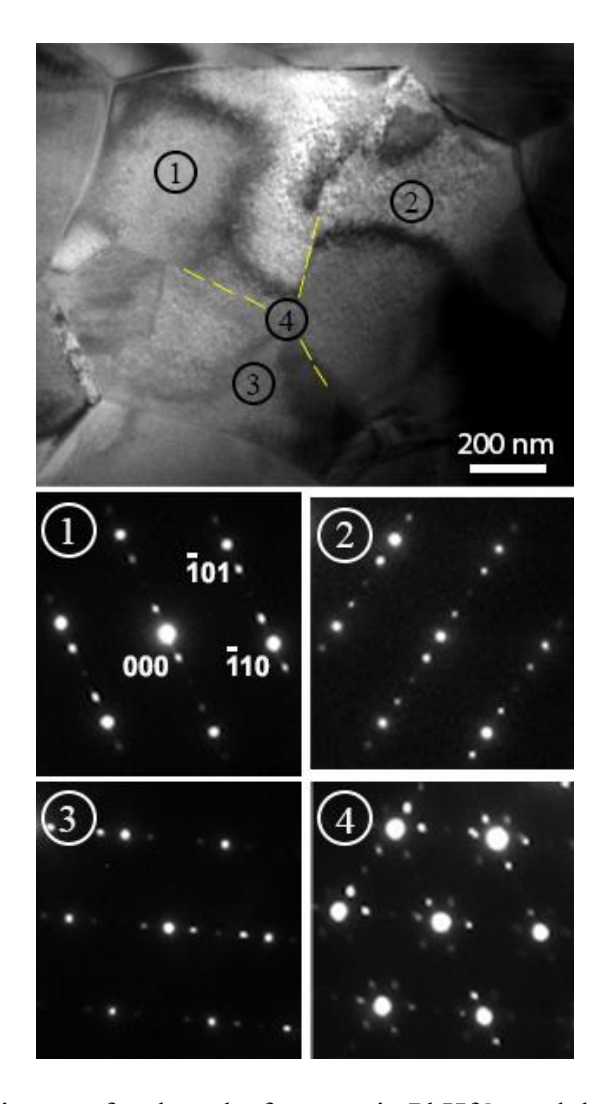


Fig. 5. TEM bright field image of a cloverleaf pattern in PbHfO₃ and the diffraction patterns recorded from the marked four different positions.

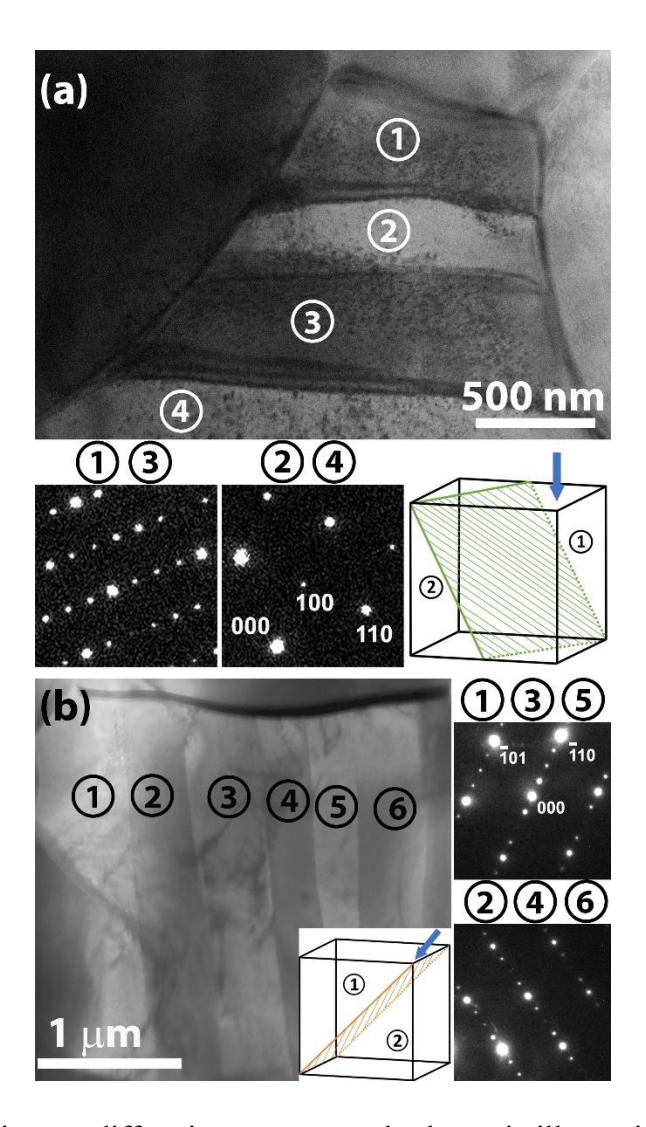


Fig. 6. The bright field image, diffraction patterns and schematic illustration of the domain walls for (a) a four-bands and (b) a six-bands lamellar pattern in PbZrO₃.

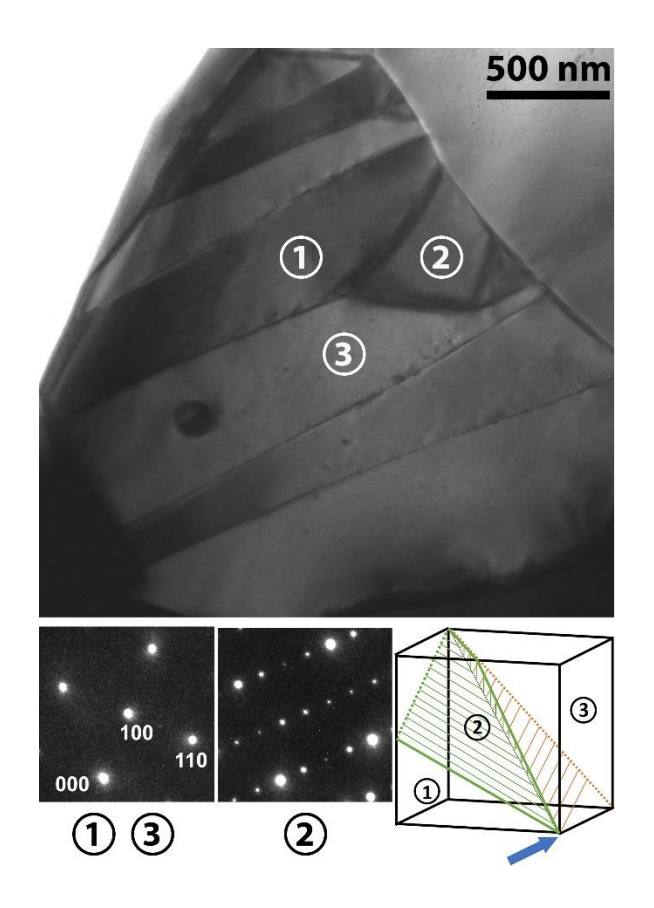


Fig. 7. A complex domain morphology in PbZrO₃ that combines a cloverleaf and a seven-bands lamellar patterns, of which the cloverleaf pattern is schematically illustrated.